ACS Combinatorial Science

RESEARCH ARTICLE

pubs.acs.org/acscombsci

High-Throughput Combinatorial Database of Electronic Band Structures for Inorganic Scintillator Materials

Wahyu Setyawan,[†] Romain M. Gaume,[‡] Stephanie Lam,[‡] Robert S. Feigelson,[‡] and Stefano Curtarolo*[,§]

[†]Department of Mechanical Engineering and Materials Science, Duke University, Durham, NC 27708,

[‡]Department of Materials Science and Engineering, Stanford University, Palo Alto, CA 94305

[§]Department of Mechanical Engineering and Materials Science and Department of Physics, Duke University, Durham, NC 27708

Supporting Information

ABSTRACT: For the purpose of creating a database of electronic structures of all the known inorganic compounds, we have developed a computational framework based on high-throughput ab initio calculations (AFLOW) and an online repository (www.aflowlib.org). In this article, we report the first step of this task: the calculation of band structures for 7439 compounds intended for the research of scintillator materials for γ-ray radiation detection. Data-mining is performed to select the candidates from 193 456 compounds compiled in the Inorganic Crystal Structure Database. Light yield and scintillation nonproportionality are predicted based on semiempirical band gaps and effective masses. We present a list of materials, potentially bright and proportional, and focus on those exhibiting small effective masses and effective mass ratios.

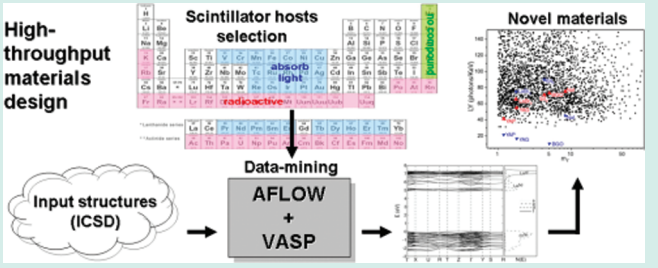

KEYWORDS: High-throughput combinatorial scintillator database, AFLOW, AFLOWLIB consortium

INTRODUCTION

The characterization of electronic band structures is an effective and efficient tool for describing materials properties, and it has become ubiquitous in solid state research.[1,2] Although a multitude of systems have been characterized in great detail, a complete database of electronic structures for all the known alloys and compounds is still missing. This can be detrimental as it hinders the search for better systems through correlative means.[3−5] To develop such a database, a distributed initiative is necessary. It requires the coordination of contributions from different scientists so that the enormous effort and outcomes can be shared. Standardization is essential to (1) minimize incorrect representations, (2) increase robustness, and (3) allow rapid information distribution.

In a recent work, we have introduced a computational framework (AFLOW) for performing high-throughput (HT) first-principle electronic structure calculations.[6] It contains the standardization of primitive cells and the symmetry paths in the reciprocal lattice for band structures of the 14 Bravais lattices, as well as the possible shapes of their Brillouin zones.[7−11]

In this article, we report our first step toward the development of such a rational database of electronic structures using a first-principle method. We start with the study of insulating inorganic compounds for nuclear applications, particularly for γ-ray radiation detection. Scintillator materials convert the high energy of γ radiation into visible photons. Typically, the number of photons per γ quanta depends the energy of the ray. The materials for which the dependence is non linear are called "nonproportional". For a radioisotope, the collection of the detected γ rays produces a pulse-height histogram. The spectrum consists of a set of bell-like curves centered at certain energies, specific for the radioisotope. Nonproportionality hinders the ability to discern different radioisotopes because it does not preserve the photons-γ intensity relationship. It is therefore crucial to understand the origin of nonproportionality for nuclear proliferation control and high-energy physics applications. In a previous study,[12] we have identified considerable band structure differences between scintillator materials that display a good proportionality of the energy response and those with poor values. This is a result of calculations on a wide variety of known scintillators and the introduction of parameters quantifying the degree of nonproportionality.[12] Effective masses of electrons at the conduction band minimum (CBM) and holes at the valence band maximum (VBM) are derived from the model band structures. The models lead to a high-throughput discovery: a surprising correlation between the nonproportionality descriptor and the ratio of electron's and hole's effective masses among the systems considered. The result, smaller mass ratios correspond to more proportional behavior. In this manuscript, we extend this approach and use the correlation to guide the data-mining process through the database. The final goal is to perform HT

Received: January 18, 2011
Revised: May 16, 2011
Published: June 06, 2011

ACS Publications © 2011 American Chemical Society

electronic structure calculations to search for future proportional and bright scintillators.

METHOD

High-Throughput Approach: AFLOW. The "Automatic Flow" (AFLOW) code[6,13−15] is our free computational materials framework that is designed to perform and manage HT calculations with minimal manual intervention. Its core HT capability can be used to invoke any external program. The fully automatic features implemented are intended for HT thermodynamics,[16−18] phonon, and electronic structure calculations[6] on top of the quantum mechanical code Vienna Ab-initio Simulation Package (VASP)[19,20] (a porting to Quantum Espresso[21] is undergoing). A complete description of AFLOW as a HT tool for automatic band structure calculations is given in reference.[6] For convenience, we give a brief summary here. AFLOW contains reliable and standardized electronic structure analysis features. It determines the symmetries, the standard conventional and primitive unit cells, the Brillouin zone (BZ) and the high-symmetry (**k**-path) for the band structure calculation, for the 14 Bravais Lattices with all of the irreducible representations. The labels and coordinates of symmetry points in the irreducible part of the Brillouin zones (IRBZ) are included. First, for a given input structure containing information about the unit cell (arbitrary) and the coordinates of atoms, AFLOW reduces it to a minimal set of basis atoms in a primitive cell (arbitrary). It then calculates the lattice and crystal symmetries to determine the space group, Bravais lattice type, and the shape variation type of the Brillouin zone. A standard conventional cell is constructed with the lattice vectors ordered according to the axial lengths and the interaxial angles. The ordering eliminates equivalent irreducible representations of some BZs in certain lattices. From the ordered standard conventional cell, a standard primitive cell is created. The standard primitive cells implemented in AFLOW are designed so that the reciprocal lattice vectors pass through the center of the Bragg planes bordering the first BZ. This choice enforces the reciprocal lattice vectors to be as perpendicular as possible to each other (Minkowski lattice reduction[22,23]) and minimizes the basis set used in plane-wave pseudopotential codes such as VASP, resulting in smaller memory requirements and faster convergence. More simply, the unique conventional cell can be seen as the reciprocal of the Minkowski lattice reduction of the reciprocal lattice. Such lattice reduction is also applied before the symmetry routine determining the space group. The symmetry points and the **k**-paths within the irreducible part of the first BZ are then constructed from the point-group of the reciprocal lattice and the potential inversions in the Bragg planes.

Moreover, AFLOW is equipped with automatic, manual (ACONVASP) and online (ACONVASP-online[6,13,14]) utilities for data extraction and I/O manipulation. Currently, it supports automatic structure selection from databases of compounds such as the Pauling File[3,24] and the Inorganic Crystal Structure Database (ICSD).[25,26] A unique structure is identified by its chemical formula and space group number. Partial occupancy of atoms is not considered at this time. Each structure is given a label which is composed of the chemical formula (alphabetically ordered by the symbol of the elements) and the original ICSD entry number. Given a list of compounds' labels, AFLOW creates a separate directory for each structure containing an input file for the intended calculation. The directories are grouped based on the Bravais lattice. Notably during the self-consistent electronic iterations in the quantum calculation, the integration over BZ is done over the irreducible part of BZ. This reduces the total number of **k**-points. Therefore, by grouping and running the structures per Bravais lattice, the usage efficiency of the computational resources can be maximized. As a HT tool, AFLOW has an option to run only one input file and then exit, to search through subfolders and to run those that have not been calculated yet, or finally to wait in the background for new structures to run. If started as a common Unix daemon through the queue of a computer cluster, AFLOW will generate, run, correct and converge a multitude of calculations per day, with minimal manual help. For managing VASP jobs, in particular, many self-healing features have been implemented. This is achieved by diagnosing the error message, self-correcting the relevant parameters, and restarting VASP. With AFLOW, a job can be easily restarted from any intermediate step. This allows users to modify input files on the fly to apply ad hoc optimization. To exploit the core HT functionality of AFLOW outside the *ab initio* program of choice, an "alien" mode is implemented. It can be used to run any external program as well as scripts for data extraction and analysis in a HT fashion. A Web site interface (ACONVASP-online)[13] is available to perform structure manipulation, symmetry recognition, and generation of the first Brillouin zone. Appropriate **k**-points labels in the irreducible part of BZ for all the **k**-paths are given online and in the original manuscript.[6]

The first-principle calculations are performed using VASP.[19,20] We use projector augmented wave pseudopotentials[27,28] and exchange-correlation functionals as parametrized by Perdew-Burke-Ernzerhof[29] within the generalized gradient approximation (GGA). Calculations are performed without zero-point motion and at zero temperature. All structures are fully relaxed. A convergence tolerance of ∼1 meV/atom is usually achieved using dense grids of 3000−4000 **k**-points per reciprocal atom for the integrations over the BZ. A much denser grid of 10 000 is employed for the static run to get accurate charge densities and density of states. The Monkhorst−Pack scheme[30,31] is used in the grid generation except for face-centered cubic, hexagonal and rhombohedral systems in which a Γ-centered grid is selected automatically by AFLOW for faster convergence. At the beginning of the structural relaxation, a spin-polarized calculation is performed for all structures. Then, if the magnetization is below 0.025 μB/atom, the spin is turned off for the next relaxations and subsequent calculations to enhance the calculation speed. In relaxing a structure to its equilibrium volume and atomic configuration, we have used large plane wave cutoff to increase basis set completeness. Throughout the calculations, the uncertainty in the pressure because of the kinetic energy cutoff of the plane waves is less than 50 MPa.

DFT+U implementation. VASP includes the DFT+U technique[32] (in our case, we use GGA+U) to enhance the on-site Coulomb interactions, which is underestimated in the density functional theory (DFT).[33] The issue arises from the DFT's inherent approximation in the exchange correlation energy that is functional of charge density rather than electronic orbitals. As expected, this approximation manifests a considerable error in strongly correlated electron systems. In VASP, Liechtenstein's[34] and Duradev's[35] implementations of GGA+U are supported. We take the latter approach as the default method in AFLOW. In this formulation, the Hubbard-like Coulomb

Table 1. List of U_{eff} Parameter Default Values in eV for the Duradev's Approach of GGA+U Approximation As Implemented in AFLOW[a]

Ti	V	Cr	Mn	Fe	Co	Ni	Cu	Zn	Ga
4.4[37]	2.7[38]	3.5[39]	4.0[39]	4.6[40]	5.0[38]	5.1[38]	4.0[39]	7.5[41]	3.9[42]
	Nb	Mo	Tc	Ru	Rh	Pd		Cd	In
	2.1[43]	2.4[43]	2.7[43]	3.0[43]	3.3[41]	3.6[41]		2.1[41]	1.9[41]
	Ta	W	Re	Os	Ir	Pt			
	2.0[43]	2.2[43]	2.4[43]	2.6[43]	2.8[43]	3.0[43]			
La	Ce	Pr	Gd	Nd	Sm	Eu	Tm	Yb	Lu
7.5[44]	6.3[45]	5.5[46]	6.0[47]	6.2	6.4	5.4	6.0[48]	6.3[49]	3.8[44]

[a] The method is applied to the 3d orbitals of the transition metal elements (top panel) and to the 4f states of the lanthanides (bottom panel).

interaction U and the screened Stoner exchange parameter J enter as an effective parameter $U_{eff} = U - J$. In the development of the database of electronic structure for scintillators, we apply the method to the 3d orbitals of the transition metal elements and to the 4f states of the lanthanides. On the basis of our experience, for La-containing compounds, the application of GGA+U is particularly important to obtain the correct states near the conduction band edge. The value for lanthanides is fit to produce the density of states of the elemental structure from the X-ray photoelectron spectroscopy and Bremsstrahlung isochromat spectroscopy (XPS-BIS) measurements.[36] Table 1 lists the default value of U_{eff} parameters used in the calculations presented in this article.

RESULTS AND DISCUSSION

Data-Mining Process. We have extracted 193 456 compounds from the ICSD structure database. Surprisingly, a significant portion of approximately 42% of the structures compiled in the ICSD database is missing at least one constituent. Considerable effort would be needed to verify whether the experimental work on these compounds is incomplete or to correct the imperfections in the data entry of the ICSD database. We proceed with the 111 950 crystalline materials that have complete constituents. Experimental determination of a crystal structure often results in partial occupations of atomic coordinates. This presents a critical challenge for computation. The size of the supercell needed to model the configuration that occurs in nature can be formidably large (>100 atoms/cell). This becomes a more serious issue for HT calculations. Hence, we are forced to exclude those systems, and we obtained 60 344 crystals that have full atomic occupancies. Following this step, redundancies due to various measurements on the same compound are removed. We obtain 34 306 unique compounds with respect to the chemical formula and the space group.

Our final database of electronic structures will contain at least 34 000 inorganic compounds. Our current priority is to select those that may be potential scintillators. For this purpose, metallic compounds are removed from the candidate list, because they absorb visible light. Furthermore, crystals containing naturally occurring radioisotopes (such as K and elements heavier than Bi) are excluded to avoid a strong signal from self-radiation. In a typical nuclear scintillation-based detection process, energy from the γ-ray radiation is converted into packets of visible photons, which are then collected using a photodetector. Hence, a critical step in designing scintillator materials consists of screening out elements which might produce absorption bands overlapping with the material's emission spectrum. The effect of crystal-field splitting on transition metals often result in various d-states with energy difference that fall in the visible spectrum. In particular, elements such as V, Cr, Mn, Fe, Co, Ni, Cu, Tc, Ru, Rh, Pd, Ag, Re, Os, Ir, Pt, and Au are known to have a strong absorption of visible light. Analogously, both spin−orbit coupling and crystal-field effects in host crystals containing Pr, Nd, Pm, Sm, Eu, Tb, Dy, Ho, Er, or Tm lead to similar optical transitions. For these reasons, compounds containing these elements as major constituents are excluded from this search. Finally, there are 12 017 compounds that pass the screening process at this point.

It is desirable to choose materials with high stopping power against γ-rays to obtain enough light within the limited size of the crystal. For an energy range below 1 MeV, the absorption is mainly due to a series of Compton scatterings and photoelectric effects. The attenuation length (μ) can be calculated from the formula mass (m_f), mass density (ρ), and the cross section of Compton (σ_c) and photoelectric (σ_{pe}) scatterings as follows:

$$\mu \equiv \frac{m_f}{\rho(\sigma_c + \sigma_{pe})} \quad (1)$$

where σ_c and σ_{pe} represent the total scattering cross sections of all atoms within the chemical formula. They can be obtained as arithmetic sums of atomic cross sections. The attenuation length can also be calculated from the volume divided by the total cross section within a unit cell. The elemental cross sections are taken from the "NIST's xcom cross section database" and references therein.[50,51] The photoelectric cross section changes more significantly as a function of γ-ray energy compared to Compton scattering. The photoelectric effect is dominant at low energy regime. For atomic numbers 10, 20, 30, 40, 50, and 60, the two cross sections become equal at about 39, 88, 145, 199, 281, and 354 keV, respectively. Any crystal containing an element that is heavier than Sc will be dominated by photoelectric absorption below 100 keV. In this study, we calculate the attenuation lengths at 511 keV, which is the energy of positron-electron annihilation utilized in medical radiology.[52] For scintillation purposes, we include only materials that exhibit $\mu < 10$ cm and we are left with 11,893 candidates in our final list. As a comparison, the attenuation lengths for familiar scintillators are 2.25 ($YAlO_3$), 1.1 ($LuAlO_3$), 2.5 (SrI_2), 4.0 (K_2LaCl_5), 3.2 (NaI), 2.3 ($LaBr_3$), and 1.1 cm (BGO). In our list, there are 8,617 compounds that have $\mu < 4$ cm. Figure 1 shows the histogram of the total attenuation length of the candidate compounds calculated using Compton scattering and photoelectric absorption cross sections data at 511 keV. A summary of the selection process is presented in Table 2.

As emphasized earlier, scintillators must be transparent to their own luminescent wavelengths. For doped materials, the band gap of the host must be larger than the transition energy of the activator. Efficient activators for scintillator materials are found in the trivalent rare earth RE^{3+} elements, such as Ce^{3+}, Pr^{3+}, Nd^{3+}, and Tb^{3+}, divalent RE^{2+}, such as Eu^{2+}, Sm^{2+}, Yb^{2+}, and Tm^{2+}, and Hg-like ions with transitions from p to s states, such as Tl^{+}, In^{+}, Ga^{+}, Pb^{2+}, Sn^{2+}, Ge^{2+}, and Bi^{3+}.[53] In the RE^{3+} group, the emission wavelength of the 5d → 4f decreases

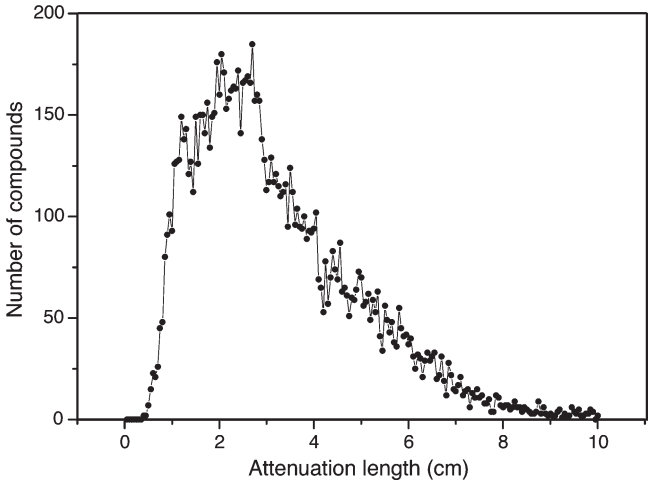

Figure 1. Histogram of total attenuation length of 11 893 candidate compounds calculated using Compton scattering and photoelectric absorption cross sections at 511 keV.

Table 2. Selection Criteria of Materials for γ-Ray Radiation Detection[a]

criterion	number of structures remaining
original list	193 456
complete basis atoms	111 950
full atom occupancy	60 344
unique compounds	34 306
nonmetallic	29 715
no radioactive or absorptive elements	12 017
μ < 10 cm	11 893
μ < 4 cm	8617

[a] The candidate compounds are extracted from the Inorganic Crystal Structure Database.[25] The total attenuation length (μ) of Compton scattering and photoelectric absorption is calculated at 511 keV.

for a given coordination as the atomic number increases because of the decrease in ionic radii, hence the stronger nucleus.[54] For example, in BaY_2F_8 crystals, the emission peak is observed around 345, 210, and 180 nm (or 3.6, 5.9, 6.9 eV) if activated using Ce^{3+}, Pr^{3+}, and Nd^{3+} ions, respectively.[55] In addition to having the smallest emission energy, Ce^{3+} also exhibits the largest probability of the 5d → 4f transition, and consequently the shortest decay time. These properties make Ce an excellent activator. The emission peak of various known Ce-activated scintillators lies near 3.4 ($YAlO_3$),[56] 3.2 ($LaBr_3$),[57] 2.9 (Lu_2SiO_5),[58] and 2.2 eV ($Y_3Al_5O_{12}$).[59] Divalent rare earth ions are mostly studied in the alkaline-earth compounds. Among these, Eu^{2+} is preferred because of its relatively high quenching temperature as compared to other RE^{2+} ions.[53] The transition energy for some Eu-activated compounds are 2.9 (CaF_2),[60] 2.8 (SrI_2),[61] and 2.6 eV (CaI_2).[62] In the Hg-like group, Tl is widely used. Tl-activated crystals emit light at 3.0 (CaI_2),[62] 3.0 (NaI),[63] and 2.2 eV (CsI).[63] Considering these emission data, we take 2, 2.5, and 2 eV as the threshold band gap of the candidates that may be activated with RE^{3+}, RE^{2+}, and Tl^{+}, respectively.

Semiempirical Band Gaps. The Kohn−Sham (KS) formalism of DFT, while leading to a correct midgap energy (Fermi level in the case of metals) with respect to vacuum,[64] underestimates the width of the gaps in semiconductors and insulators. For the exact KS formalism, the physical gap is equal to the KS gap plus the derivative discontinuity of the exchange-correlation (xc) energy with respect to the number of electrons.[64−66] In a nonexact KS approach with an approximate xc energy functional, the above relation may not be exact and in addition, the approximate functional may not reproduce the correct xc energy derivatives.[67,68] Several correction techniques such as the GGA+U applied in this work (even though it can predict the correct orbitals near the CBM and VBM) can improve the KS gap only to a limited extent. A new semiempirical method to estimate the band gap within the standard DFT has been recently introduced.[69] It is named Δ-sol method as it is based on the delta self-consistent-field (Δ-SCF) theory.[1] It requires the evaluation of the total energy at three different numbers of electrons (N, $N + \delta$, and $N - \delta$), N being the number of electrons in the neutral ground state. δ represents the amount of added or removed charge to simulate the excitation process. It depends on N and is determined empirically to best yield the experimental band gap. In a unit cell with periodic boundary conditions, the introduction of an additional charge results in an additional term in the total energy due to charge−image interactions. Unfortunately, the determination of charge−image correction requires the calculation of the electronic dielectric constant to account for the screening effect. This calculation takes more than an order of magnitude longer than the standard DFT and hence is not suitable for the HT approach. We perform a simulation to study the accuracy of Δ-sol method when the charge−image correction is not applied. We gather over a hundred compounds with known experimental gaps spanning from ∼1 to 12 eV as listed in Table 3.[53,70] The result is shown in Figure 2, in which we plot the experimental gaps versus the Kohn−Sham gaps and the Δ-sol gaps. A linear least-squares fit gives $E_g^{exp} = 1.348E_g^{KS} + 0.913$ with $R^2 = 0.890$ and $E_g^{exp} = 1.349E_g^{\Delta\text{-sol}} - 0.429$ with $R^2 = 0.886$. Both data exhibit a similar fit quality and interestingly also a similar slope of the fit lines. For the KS gaps, the root-mean-square (rms) of the percentage error is 42%, which can be reduced to 24% if we use the fitted values. For the Δ-sol case, even though the rms of the absolute error is reduced, the percentage error remains unchanged (27% without fit and 28% using the fitted values). This study shows that even though the Δ-sol improves the accuracy of the KS gaps, it does not necessarily perform better than a direct-empirical fitted values of KS gaps. Therefore, for our current study, we adjust the KS gaps according to the KS empirical line and denote the fitted gap as E_{gfit}. To characterize the issue of overfitting, we have performed the two extremes of the k-fold cross-validation method.[71] The leave-one-out technique yields an overall average of rms error of 0.933 eV. This value is 1.8% larger than the rms error of the LSQ model which is 0.916 eV. The other extreme is the 2-fold cross-validation. In this method, the average rms error over 2 million samples is 0.942 eV (approximately 2.8% larger than the LSQ error). Thus, we expect that our LSQ model overfits for less than ∼3%.

A large band gap does not necessarily imply that the materials can be activated with a certain dopant. The relative position of the transition states below the host's conduction band minimum (CBM) and above the valence band maximum (VBM) is crucial. For example, in the Ce-activated materials, the 5d level must be below CBM and the energy difference (δE_e) should be larger than the thermal energy to avoid thermal excitation of the

Table 3. List of Compounds with Known Experimental Band Gaps Ranging from ∼1 to 12 eV That Are Used for Empirical Adjustment of the Calculated Gaps[a]

IA−IIA	IIA−VIIA	IIA−VIA	IIIA−VIA
LiF, LiCl, LiBr, LiI, NaF, NaCl, NaBr, NaI, KF, KCl, KBr, KI, RbF, RbCl, RbBr	MgF_2, $MgCl_2$, $MgBr_2$, CaF_2, $CaCl_2$, CaI_2, SrF_2, $SrCl_2$, BaF_2, $BaCl_2$	BeO, MgO, MgSe, MgTe, CaO, CaS, CaSe, CaTe, SrO, SrS, SrSe, SrTe, BaO, BaS, BaSe, BaTe	Al_2O_3, Al_2Se_3, Al_2Te_3, Ga_2O_3, Ga_2S_3, Ga_2Se_3, In_2O_3RbI, CsF, CsCl, CsBr, CsI
IVA-VIA:	early(d)-p:	late(d)-p:	other:
SiO_2, $SiSe_2$, GeO_2, GeS_2, $GeSe_2$, SnO_2, SnS_2, $SnSe_2$	Sc_2O_3, Y_2O_3, TiO_2, ZrO_2, ZrS_2, HfO_2, Nb_2O_5, Ta_2O_5, MoO_3, MoS_2, WO_3, WSe_2, YF_3, LaF_3, CeO_2,CeF_3	CuCl, CuBr, ZnO, ZnS, ZnSe, ZnTe, CdS, CdSe, CdTe, Cu_2O	BiI_3, $YAlO_3$, $LuAlO_3$, $LaAlO_3$, $Bi_4Ge_3O_{12}$, $PbWO_4$, $SrTiO_3$, $LiNbO_3$, $LiIO_3$, $LiYF_4$,AlAs, GaN, GaP, Si_3N_4, Na_2Se, Na_2Te

[a] The compounds are grouped according to the valence electrons. The experimental data are gathered from references.[53,70].

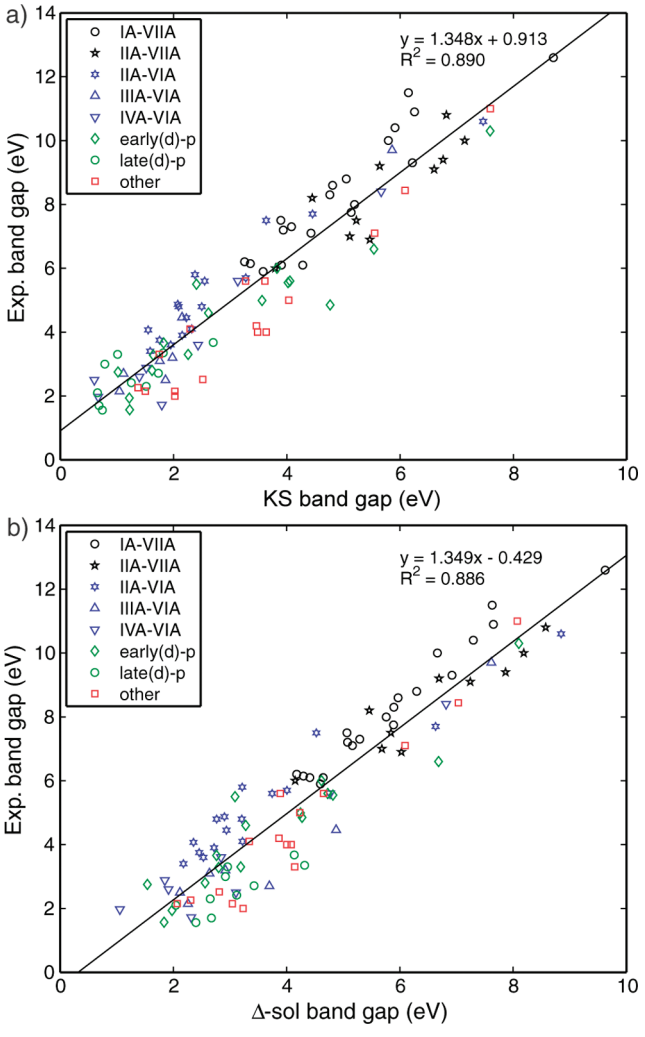

Figure 2. Experimental band gaps vs (a) Kohn−Sham DFT gaps and (b) Δ-sol DFT gaps.[69] The root-mean-square error in the Kohn−Sham case is reduced from 42% to 24% by using the fitted values, while it remains constant at 27% in the second case.

electron back to the conduction band. On the other hand, too large a δE_e would decrease the probability of Ce^{3+} to capture an electron since it has to compete with the defect levels, which act as electrons traps. In addition, more phonon modes would need to be available to dissipate large δE_e, further reducing the probability of electron capture. A similar situation applies for the hole, in which the Ce's 4f level should be above the VBM, and this energy difference (δE_h) should also be optimal. Note that if the excitation of the Ce atom is mediated by a capture of an exciton, δE_e and δE_h play a less critical role. Another important factor is the localization of the excited state of cerium (Ce*). Successful scintillation would require a high degree of localization of the Ce* state.[72] To study the dopant levels and their localization, a relevant size of the supercell is needed. It imposes even more demanding computational resources which is not suited for HT method. Nevertheless, we enforce the following criteria to increase the likelihood of successful activation. These include comparing the atomic sizes and valences for possible substitutional doping. With these requirements and the band gap sizes, we divide the results into four groups: RE^{3+}-activated (group A), RE^{2+}-activated (group B), Tl^{+}-activated (group C), and an additional group (D). In group D, we include all the materials that do not belong to groups A, B, or C. The results are compiled in the Supporting Information. The data are arranged with increasing m_r. The total number of compounds is 2859.

In the Supporting Information, we present the data which include the chemical formula, the ICSD entry number, the space group number, the Pearson symbol, the experimental mass density, the KS band gaps (E_g), the gap type (I, indirect; D, direct), the fitted KS band gaps (E_{gfit}), the width of the valence band (E_{vw}), the gap between the valence band and the lower valence band (E_{gcv}), the effective mass of electrons near CBM (m_e), the minimum value min(m_e), the effective mass of holes near VBM (m_h), the minimum value min(m_h), the ratio of the effective masses (m_r), and the attenuation length (μ) at 511 keV. Band structures and density of states pictures are available online.[15]

The effective masses are computed using the following algorithm. All unique symmetry paths in the IRBZ are included in the band structure data. Using a tolerance of 26 meV relevant to ambient temperature, the extrema corresponding to the CBM and VBM are identified. In most cases, there are more than one segment within the **k**-path that constitute the extrema (sum over segment). For example, in orthorhombic systems, if the CBM occurs at point Γ, there will be three contributions to m_e resulting from the X−Γ−X, Y−Γ−Y, and Z−Γ−Z segments. In addition, in each segment, there may be more than one band that falls within the 26 meV tolerance. These would make additional contributions to the average m_e (sum over bands). Next, we take

into account the contributions resulting from the equivalent segments that are omitted in the **k**-path during band structure calculation. They need to be accounted for because the locations of the extreme **k**-points will be different in space (sum over the IRBZ). Finally, to account for all the coordinates of the extreme **k**-points and all the included segments, we apply the point symmetry operations of the reciprocal lattice to get the complete contributions from the full BZ (sum over point symmetry). Note that the last step is needed because the multiplicity of the segment is not always the same (in fact, it is different in most cases) as the multiplicity of the **k**-point with respect to point symmetry operations. Consequently, the average over IRBZ in most cases differs from that over the full BZ. The final average of electron's effective mass m_e (similar steps apply for determining hole's effective mass average m_h) can be summarized with the following equation:

$$m_e = \text{average}\left(\sum_{i}^{k\text{-segment}} \sum_{j}^{\text{bands}} \sum_{k}^{\text{IRBZ}} \sum_{l}^{\text{point sym}} m_{e,ijkl}\right) \quad (2)$$

The individual band mass $m_{e,ijkl}$ is derived from the inverse of the second derivatives of the Kohn−Sham eigenvalues with respect to the wave vector **k**. The effective mass ratio m_r is then defined as

$$m_r = \max\left(\frac{m_h}{m_e}, \frac{m_e}{m_h}\right) \quad (3)$$

The definition measures the similarity between the electron's mass and the hole's mass. In our previous study,[12] we report on our observation that there exists a correlation between m_r and the nonproportionality response in various scintillators crystals. Notably, a smaller ratio (closer to 1) leads to a more proportional behavior. This applies particularly for compounds in which free electrons and holes constitute the dominant energy carriers, such as in Ce:$YAlO_3$, Ce:$Y_3Al_5O_{12}$, Ce:Y_2SiO_5, and BGO. This finding is consistent with a recent work on the role of hole mobility in scintillator nonproportionality.[73] The diffusion and drift motion of free charges is governed by the chemical potential and Coulomb force, respectively. The diffusion term is linear with the charge concentration, while the drift is quadratic (a product of charge density and the self-electric field). The nonproportionality is believed to be rooted mainly in the loss of energy carriers experience because of nonradiative processes, such as Auger recombination and deep level trapping. Several scenarios can be thought of as follows:

(1) At the beginning of ionization track (low carrier concentration) and large m_r: Diffusion is dominant, there is a large separation between electrons and holes and large nonproportionality.

(2) For the case of low carrier concentration and small m_r: Diffusion is still dominant but there is a small separation of the electrons and holes and a small nonproportionality.

(3) At the end of ionization track (high carrier concentration) and with a large m_r: Drift is dominant. The more immobile carriers will keep the more mobile counterparts within a small charge region, nonradiative Auger formation becomes important and nonproportionality increases.

(4) For the case of high carrier concentration and small m_r: Drift is dominant and electrons and holes are close together. If both carriers are mobile, they will populate a relatively large charge region, reducing the probability of the Auger process and thereby decreasing nonproportionality.

It is then advantageous to have a small m_r, particularly with mobile electrons and holes. An interesting case is when m_r is small, but both m_e and m_h are large. In this case, even though the Auger process plays an important role, the Auger formation rate is expected to be smaller than in the case in which one of the carriers is mobile, allowing scintillation to successfully occur. Hence, good proportionality can still be expected.

Band gap energy can be used to estimate the light yield (LY) using the relation:

$$\text{LY} = \frac{\alpha N_{eh}}{E_\gamma} = \frac{\alpha}{\beta E_g} \times 1000\ [\text{ph/keV}] \quad (4)$$

where E_γ is the deposited γ-ray energy, N_{eh} is the number of excited electron−hole (e−h) pairs, and α is the conversion factor from e−h pairs (or excitons) to visible photons. Because of energy losses, the amount of energy to create an e−h pair (E_{eh}) during the carrier production is larger than the band gap by a factor β. The average E_{eh} is a sum of the gap (E_g), mean kinetic energies of electrons (E_e) and holes (E_h) during thermalization, and the energy of phonons (E_{ph}) generated from the excess energy of the carriers above the ionization threshold (E_t):

$$E_{eh} = E_g + E_e + E_h + E_{ph} \quad (5)$$

Assuming a parabolic band dispersion and a uniform distribution of electrons in the conduction band, $E_e = 0.6E_t$.[53] By applying the conservation of energy and momentum in the second generation of e−h pair production, the threshold energy is given by

$$E_t = \left(\frac{1 + 2m_e/m_h}{1 + m_e/m_h}\right) E_g \quad (6)$$

The minimum β that gives the maximum LY can be calculated by taking $E_{ph} = 0$

$$E_{eh} = E_g + 0.6E_t + 0.6E_t \quad (7)$$

$$\beta = \frac{E_{eh}}{E_g} = 1 + 1.2\left(\frac{1 + 2m_e/m_h}{1 + m_e/m_h}\right) \quad (8)$$

In the above formula, we make a further approximation that the average kinetic energies of the holes is the same as that of electrons. The carriers-to-photons conversion factor α varies across different materials. It also depends on the temperature and the quality of the materials (defects, impurities, homogeneities, etc). Nevertheless, the maximum LY can be calculated by taking $\alpha = 1$. Figure 3a shows a plot of the predicted maximum LY versus ratio of the effective mass, generated by using E_{gfit} as E_g. In Figure 3a, theoretical (red triangles) and experimental (blue triangles) LYs for several familiar scintillators are included for comparison. The reported LYs for BGO, NaI and YAG are significantly lower than the maximum predicted. The large discrepancies are due to the large deviation of α at room temperature from the ansatz unit value. Indeed, the low-temperature measurements of LY for pure NaI at 77 K and BGO at 170 K are 76 and 68 ph/keV.[74] They compare well with the predicted values of 75 and 73 ph/keV. Nevertheless, we note that the model should not be used to draw comparisons with experimental measurements. It should be rather used as a general guide for expecting maximum LYs. The predicted LYs for the

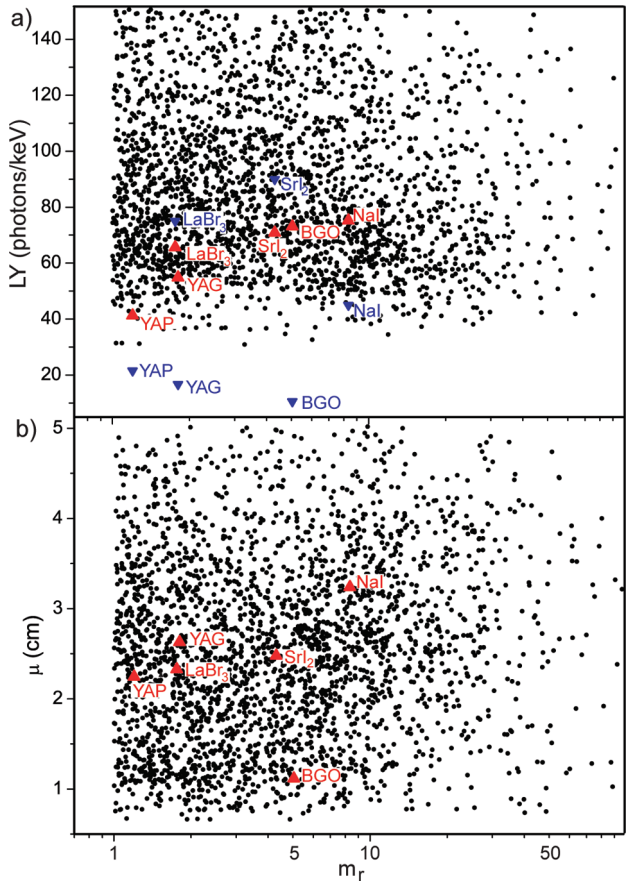

Figure 3. Data plot of 2859 compounds showing (a) predicted maximum light yield (LY) and (b) the total Compton and photoelectric attenuation length (μ) vs the ratio of electron's and hole's effective mass (m_r). The data points for several familiar scintillators are included for comparison (red triangles). Their experimental LYs are denoted by blue triangles in a.

reference scintillators fall mostly between 40 and 80 ph/keV. A good population of candidates exists in the region of predicted LY higher than 40 ph/keV. The corresponding plot for attenuation length versus m_r is given in Figure 3b).

CONCLUSION

On the basis of the strategy described above, we may select candidate scintillator materials that are expected to be bright and proportional by choosing those with a small band gap (light yield is inversely proportional to E_g), small m_e, m_h, and m_r. Using the Supporting Information one may find a good number of compounds with those properties. For example: Y_2OS_2 (SG#14, mP20), Gd_2O_2Se (SG#164, hP5), $Cs_3Y_2I_9$ (SG#194, hP28), Ba_2BiTaO_6 (SG#148, hR10), $TlSbO_3$ (SG#182, hP20), and $PbAs_2O_6$ (SG#162, hP9). For monoclinic Y_2OS_2, substituting Y with RE atoms changes the electronic structure only slightly. This is also true in the hexagonal families of RE-oxysulfides and RE-oxyselenides. Even though there are many promising candidates reported in this work, more detailed studies are needed to corroborate the results. Nevertheless, the model can be seen as a practical guide to reduce the number of expensive and time-consuming experimental validations. Regardless of the approximations within the AFLOW high-throughput approach, the overall validity of the method will be established by guided experimental findings, which are subject of our future effort.

The computational framework and data-mining procedure presented in this paper can be applied and adapted for other materials applications. In synergy with other researchers, the database of electronic structures will grow toward the goal of containing all the compounds of technological interest, similar to what we are currently conducting for the database of binary alloys.[75,16]

ASSOCIATED CONTENT

Supporting Information. Electronic structure data of selected potential scintillators. This material is available free of charge via the Internet at http://pubs.acs.org.

AUTHOR INFORMATION

Corresponding Author

*E-mail: stefano@duke.edu.

Funding Sources

This work is supported in part by the Department of Homeland Security—Domestic Nuclear Detection Office, by the Office of Naval Research (N00014-07-1-0878, N00014-07-1-1085, N00014-09-1-0921), and by the National Science Foundation (DMR-0639822). We are grateful for extensive use of the Teragrid resources (MCA-07S005).

ACKNOWLEDGMENT

The authors acknowledge Ohad Levy, Gus L. W. Hart, Roman Chepulskyy, Michal Jahnatek, Shidong Wang, Marco Buongiorno-Nardelli, and Natalio Mingo for fruitful discussions.

REFERENCES

(1) Martin, R. M. *Electronic Structure: Basic Theory and Practical Methods*; Cambridge University Press: Cambridge, England, 2004.

(2) Hafner, J. Ab-initio simulations of materials using VASP: density-functional theory and beyond. *J. Comput. Chem.* **2008**, *29*, 2044.

(3) Villars, P.; Berndt, M.; Brandenburg, K.; Cenzual, K.; Daams, J.; Hulliger, F.; Massalski, T.; Okamoto, H.; Osaki, K.; Prince, A.; Putz, H.; Iwata, S. The Pauling file, Binaries edition. *J. Alloys Compd.* **2004**, *367*, 293–297.

(4) Nørskov, J. K.; Bligaard, T.; Rossmeisl, J.; Christensen, C. H. Towards the computational design of solid catalysts. *Nat. Chem.* **2009**, *1*, 37–46.

(5) Nørskov, J. K.; Abild-Pedersen, F. Catalysis: Bond control in surface reactions. *Nature* **2009**, *461*, 1223–1225.

(6) Setyawan, W.; Curtarolo, S. High-throughput electronic band structure calculations: Challenges and tools. *Comput. Mater. Sci.* **2010**, *49*, 299.

(7) Kovalev, O. V. *Irreducible Representations of the Space Groups*; Gordon and Breach: New York, 1965.

(8) Miller, S. C.; Love, W. F. *Tables of Irreducible Representations of Space Groups and Co-Representations of Magnetic Groups*; Pruett Press: Boulder, CO, 1967.

(9) Casher, A.; Glucky, M.; Gur, Y. *The Irreducible Representations of Space Groups*; W. A. Benjamin Inc.: New York, 1969.

(10) Bradley, C. J.; Cracknell, A. P. *the Mathematical Theory of Symmetry in Solids: Representation Theory for Point Groups and Space Groups*; Clarendon Press: Oxford, U.K., 1972.

(11) Burns, G.; Glazer, A. M. *Space Groups for Solid State Scientists*; Academic Press: Boston, 1990.

(12) Setyawan, W.; Gaume, R. M.; Feigelson, R. S.; Curtarolo, S. Comparative study of nonproportionality and electronic band structures features in scintillators materials. *IEEE Trans. Nucl. Sci.* **2009**, *56*, 2989.
(13) Curtarolo, S.; Hart, G. L. W.; Setyawan, W.; Mehl, M.; Jahnatek, M.; Chepulskii, R. V.; Levy, O.; Morgan, D. AFLOW: software for high-throughput calculation of material properties, http://materials.duke.edu/aflow.html, 2010.
(14) Curtarolo, S.; Setyawan, W.; Hart, G. L. W.; Jahnatek, M.; Chepulskii, R. V.; Taylor, R. H.; Wang, S.; Xue, J.; Yang, K.; Levy, O.; Mehl, M.; Morgan, D. AFLOW: An automatic framework for high-throughput quantum mechanical materials discovery. **2011**, submitted.
(15) Setyawan, W.; Curtarolo, S. Database of electronic band structures for inorganic scintillator materials, http://www.aflowlib.org.
(16) Levy, O.; Hart, G. L. W.; Curtarolo, S. Uncovering compounds by synergy of cluster expansion and high-throughput methods. *J. Am. Chem. Soc.* **2010**, *132*, 4830.
(17) Levy, O.; Chepulskii, R. V.; Hart, G. L. W.; Curtarolo, S. New face of rhodium alloys: Revealing ordered structures from first principles. *J. Am. Chem. Soc.* **2010**, *132*, 833.
(18) Taylor, R.; Curtarolo, S.; Hart, G. L. W. Predictions of the Pt_8Ti phase in unexpected systems. *J. Am. Chem. Soc.* **2010**, *132*, 6851.
(19) Kresse, G.; Hafner, J. Ab initio molecular dynamics for liquid metals. *Phys. Rev. B* **1993**, *47*, 558–561.
(20) Kresse, G.; Furthmuller, J. Efficiency of ab initio total energy calculations for metals and semiconductors using a plane-wave basis set. *Comput. Mater. Sci.* **1996**, *6*, 15.
(21) Giannozzi, P.; et al. QUANTUM ESPRESSO: A modular and open-source software project for quantum simulations of materials. *J. Phys.: Condens. Matter.* **2009**, *21*, 395502.
(22) Nguyen, P. Q.; Stehle, D. Low-dimensional lattice basis reduction revisited. *ACM Trans. Alg.* **2009**, *5*, 1.
(23) Minkowski, H. *Geometrie der Zahlen*; Teubner-Verlag: Leipzig, 1896.
(24) Villars, P.; Cenzual, K.; Daams, J. L. C.; Hulliger, F.; Massalski, T. B.; Okamoto, H.; Osaki, K.; Prince, A.; Iwata, S. *Crystal Impact, Pauling File. Inorganic Materials Database and Design System, Binaries ed.*; ASM International: Metal Park, OH, 2003.
(25) Mighell, A. D.; Karen, V. L. NIST materials science databases. *Acta Crystallogr.* **1993**, *A49*, c409.
(26) Karlsruhe, F. Inorganic Crystal Structure Database, http://icsd.fiz-karlsruhe.de/icsd/.
(27) Blöchl, P. E. Projector augmented-wave method. *Phys. Rev. B* **1994**, *50*, 17953.
(28) Kresse, G.; Joubert, D. From ultrasoft pseudopotentials to the projector augmented-wave method. *Phys. Rev. B* **1999**, *59*, 1758.
(29) Perdew, J. P.; Burke, K.; Ernzerhof, M. Generalized gradient approximation made simple. *Phys. Rev. Lett.* **1996**, *77*, 3865–3868.
(30) Monkhorst, H. J.; Pack, J. D. Special points for Brillouin-zone integrations. *Phys. Rev. B* **1976**, *13*, 5188–5192.
(31) Pack, J. D.; Monkhorst, H. J. "Special points for Brillouin-zone integrations"—A reply. *Phys. Rev. B* **1977**, *16*, 1748–1749.
(32) Anisimov, V. I.; Aryasetiawan, F.; Lichtenstein, A. I. First-principles calculations of the electronic structure and spectra of strongly correlated systems: The LDA + U method. *J. Phys.: Condens. Matter.* **1997**, *9*, 767.
(33) Kohn, W.; Sham, L. J. Self-consistent equations including exchange and correlation effects. *Phys. Rev.* **1965**, *140*, A1133.
(34) Liechtenstein, A. I.; Anisimov, V. I.; Zaanen, J. Density-functional theory and strong interactions: Orbital ordering in Mott–Hubbard insulators. *Phys. Rev. B* **1995**, *52*, R5467.
(35) Duradev, S. L.; Botton, G. A.; Savrasov, S. Y.; Humphreys, C. J.; Sutton, A. P. Electron-energy-loss spectra and the structural stability of nickel oxide: An LSDA+U study. *Phys. Rev. B* **1998**, *57*, 1505.
(36) Lang, J. K.; Baer, Y.; Cox, P. A. Study of the 4f and valence band density of states in rare-earth metals. II. Experiment and results. *J. Phys. F: Met. Phys.* **1981**, *11*, 121.
(37) Cuong, D. D.; Lee, B.; Choi, K. M.; Ahn, H.-S.; Han, S.; Lee, J. Oxygen vacancy clustering and electron localization in oxygen-deficient $SrTiO_3$: LDA+U study. *Phys. Rev. Lett.* **2007**, *98* No. 115503.
(38) Pickett, W. E.; Erwin, S. C.; Ethridge, E. C. Reformulation of the LDA+U method for a local-orbital basis. *Phys. Rev. B* **1998**, *58*, 1201.
(39) Wang, L.; Maxisch, T.; Ceder, G. Oxidation energies of transition metal oxides within the GGA+U framework. *Phys. Rev. B* **2006**, *73*, 195107.
(40) Cococcioni, M.; de Gironcoli, S. Linear response approach to the calculation of the effective interaction parameters in the LDA+U method. *Phys. Rev. B* **2005**, *71*, No. 035105.
(41) Erhart, P.; Albe, K.; Klein, A. First-principles study of intrinsic point defects in ZnO: Role of band structure, volume relaxation, and finite-size effects. *Phys. Rev. B* **2006**, *73*, No. 205203.
(42) Janotti, A.; Segev, D.; de Walle, C. G. V. Effects of cation d states on the structural and electronic properties of III-nitride and II-oxide wide-band-gap semiconductors. *Phys. Rev. B* **2006**, *74*, No. 045202.
(43) Solovyev, I. V.; Dederichs, P. H.; Anisimov, V. I. Corrected atomic limit in the local-density approximation and the electronic structure of d impurities in Rb. *Phys. Rev. B* **1994**, *50*, No. 16861.
(44) Wegner, D.; Bauer, A.; Koroteev, Y. M.; Bihlmayer, G.; Chulkov, E. V.; Echenique, P. M.; Kaindl, G. Surface electronic structures of La(0001) and Lu(0001). *Phys. Rev. B* **2006**, *73*, No. 115403.
(45) Jiang, Y.; Adams, J. B.; van Schilfgaarde, M. Density-functional calculation of CeO_2 surfaces and prediction of effects of oxygen partial pressure and temperature on st abilities. *J. Chem. Phys.* **2005**, *123*, No. 064701.
(46) Harima, H. LDA+U method applied for f-electron systems. *J. Magn. Magn. Mater.* **2010**, *226*, 83.
(47) Harmon, B. N.; Antropov, V. P.; Liechtenstein, A. I.; Solovyev, I. V.; Anisimov, V. I. Calculation of magneto-optical properties for 4f systems: LSDA + Hubbard U results. *J. Phys. Chem. Solids* **1995**, *56*, 1521.
(48) Antonov, V. N.; Harmon, B. N.; Yaresko, A. N. Electronic structure and magneto-optical Kerr effect of Tm monochacogenides. *Phys. Rev. B* **2001**, *63*, No. 205112.
(49) Jeong, T. Electronic structure and magnetism of antiferromagnetic heavy fermion compound YbSi. *J. Phys.: Condens. Matter* **2006**, *18*, 6769.
(50) Berger, M. J.; Hubbell, J. H.; Seltzer, S. M.; Chang, J.; Coursey, J. S.; Sukumar, R.; Zucker, D. S.; Olsen, K. XCOM: Photon Cross Sections Database, http://www.nist.gov/pml/data/xcom/index.cfm, 1998.
(51) Scofield, J. H. Theoretical photoionization cross sections from 1 to 1500 keV. *Lawrence Livermore Lab., [Rep.] UCRL* **1973**No. UCRL-51326.
(52) Knoll, G. F. *Radiation Detection and Measurement*; John Wiley and Sons: New York, 2000.
(53) Rodnyi, P. A. *Physical Processes in Inorganic Scintillators*; CRC Press: New York, 1997.
(54) Schlesinger, M.; Szczurek, T. 4f to 5d transition studies of some rare-earth ions in CaF_2. *Phys. Rev. B* **1973**, *8*, 2367.
(55) Chernov, S. P.; Devyatkova, L. I.; Ivanova, O. N.; Kaminskii, A. A.; Mikhailin, V. V.; Rudnev, S. N.; Uvarova, T. V. $5d^14f^{N-1}$-$4f^N$ absorption and luminescence of Ce^{3+}, Pr^{3+}, and Nd^{3+} ions in BaY_2F_8. *Phys. Status Solidi A* **1985**, *88*, K169.
(56) Lempicki, A.; Randles, M. H.; Wisniewski, D.; Balcerzyk, M.; Brecher, C.; Wojtowicz, A. J. $LuAlO_3$-Ce and other aluminate scintillators. *IEEE Trans. Nucl. Sci.* **1995**, *42*, 280.
(57) van Loef, E. V. D.; Dorenbos, P.; van Eijk, C. W. E.; Kramer, K. W.; Gudel, H. U. Scintillation properties of $LaBr_3$:Ce^{3+} crystals: fast, efficient and high-energy-resolution scintillators. *Nuc. Instrum. Methods Phys. Res., Sect. A* **2002**, *486*, 254.
(58) Melcher, C. L.; Schweitzer, J. S. Cerium-doped lutetium oxyorthosilicate—A fast, efficient new scintillator. *IEEE Trans. Nucl. Sci.* **1992**, *39*, 502.
(59) Mihokova, E.; Nikl, M.; Mares, J. A.; Beitlerova, A.; Vedda, A.; Nejezchleb, K.; Blazek, K.; D'Ambrosio, C. Luminescence and scintillation properties of YAG:Ce single crystal and optical ceramics. *J. Lumin.* **2007**, *126*, 77.

(60) Kobayasi, T.; Mroczkowski, S.; Owen, J. F.; Brixner, L. H. Fluorescence lifetime and quantum efficiency for 5d−4f transitions in Eu^{2+}-doped chloride and fluoride crystals. *J. Lumin.* **1980**, *21*, 247.
(61) Cherepy, N. J.; Hull, G.; Drobshoff, A. D.; Payne, S. A.; Loef, E. V.; Wilson, C. M.; Shah, K. S.; Roy, U. N.; Burger, A.; Boatner, L. A.; Choong, W. S.; Moses, W. W. Strontium and barium iodide high light yield scintillator. *Appl. Phys. Lett.* **2008**, *92*, 083508.
(62) Hofstadter, R.; Odell, E. W.; Schmidt, C. T. $CaI_2 + CaI_2(Eu)$ Scintillation Crystals. *Rev. Sci. Instrum.* **1964**, *35*, 246.
(63) Haas, J. T. M.; Dorenbos, P. Advances in yield calibration of scintillators. *IEEE Trans. Nucl. Sci.* **2008**, *55*, 1086.
(64) Perdew, J. P.; Levy, M. Physical content of the exact Kohn−Sham orbital energies: Band gaps and derivatives discontinuities. *Phys. Rev. Lett.* **1983**, *51*, 1884.
(65) Sham, L. J.; Schluter, M. Density functional theory of the energy gap. *Phys. Rev. Lett.* **1983**, *51*, 1888.
(66) Janak, J. F. Proof that $dE/dn_i = \varepsilon_i$ in density functional theory. *Phys. Rev. B* **1978**, *18*, 7165.
(67) Cohen, A. J.; Mori-Sánchez, P.; Yang, W. Fractional charge perspective on the band gap in density-functional theory. *Phys. Rev. B* **2008**, *77*, 115123.
(68) Mori-Sánchez, P.; Cohen, A. J.; Yang, W. Localization and delocalization errors in density functional theory and implications for band-gap prediction. *Phys. Rev. Lett.* **2008**, *100*, 146401.
(69) Chan, M. K. Y.; Ceder, G. Efficient band gap prediction for solids. *Phys. Rev. Lett.* **2010**, *105*, 196403.
(70) Weber, M. J. *Handbook of Optical Materials*; CRC Press: New York, 2002.
(71) Mosteller, F.; Turkey, J. W. *Data Analysis, Including Statistics. In Handbook of Social Psychology*; Addison-Wesley: Reading, MA, 1968.
(72) Canning, A.; Boutchko, R.; Chaudhry, A.; Derenzo, S. E. First-principles studies and predictions of scintillation in Ce-doped materials. *IEEE Trans. Nucl. Sci.* **2009**, *56*, 944.
(73) L., Q.; Grim, J. Q.; Williams, R. T.; Bizarri, G. A.; Moses, W. W. The role of hole mobility in scintillator proportionality. *Nucl. Instrum. Methods Phys. Res., Sect. A* **2010**10.1016/j.nima.2010.07.074.
(74) Derenzo, S. E.; Moses, W. W. Experimental efforts and results in finding new heavy scintillators. In *Proceedings of the Crystal 2000 International Workshop "Heavy Scintillators for Scientific and Industrial Applications*; Frontieres: Gif-sur-Yvette Cedex, France, 1993; p 125.
(75) Curtarolo, S.; Morgan, D.; Ceder, G. Accuracy of ab initio methods in predicting the crystal structures of metals: Review of 80 binary alloys. *CALPHAD* **2005**, *29*, 163.

NOTE ADDED AFTER ASAP PUBLICATION

Reference 14 was incorrect in the version of this paper published June 16, 2011. The correct version published June 23, 2011.